Обзор ArXiv/astro-ph, 1-4 сентября 2020

От Сильченко О.К.

ArXiv:2009.01112

The WISSH QSOs project

IX. Cold gas content and environment of luminous QSOs at Cosmic noon

M. Bischetti[1,2] ⋆, C. Feruglio[1], E. Piconcelli[2], F. Duras[3,2], M. Pérez-Torres[4,5], R. Herrero[6,7], G. Venturi[8], S. Carniani[9], G. Bruni[10], I. Gavignaud[11], V. Testa[2], A. Bongiorno[2], M. Brusa[12,13], C. Circosta[14], G. Cresci[15], V. D'Odorico[1,9], R. Maiolino[16,17], A. Marconi[18,15], M. Mingozzi[19], C. Pappalardo[20], M. Perna[21,15], E. Traianou[22], A. Travascio[2], G. Vietri[23], L. Zappacosta[2], and F. Fiore[1]

(Affiliations can be found after the references)

ABSTRACT

Context. Sources at the brightest end of the QSO luminosity function ($L_{\rm Bol} > 10^{47}$ erg s^{-1}) during the peak epoch in the history of star formation and black hole accretion ($z \sim 2-4$, often referred to as "Cosmic noon") are privileged sites to study the *feeding & feedback* cycle of massive galaxies.

Aims. We aim to perform the first systematic study of cold gas properties in the most luminous QSOs, by characterising their host-galaxies and environment. These targets exhibit indeed widespread evidence of outflows at nuclear and galactic scales.

Methods. We analyse ALMA, NOEMA and JVLA observations of the far-infrared continuum, CO and [CII] emission lines in eight QSOs (bolometric luminosity $L_{\rm Bol} \gtrsim 3 \times 10^{47}$ erg s^{-1}) from the WISSH sample at $z \sim 2.4-4.7$.

Results. We report a 100% emission line detection rate and a 80% detection rate in continuum emission, and we find CO emission to be consistent with the steepest CO ladders observed so far. Sub-millimetre data reveal widespread presence of (one or more) bright companion galaxies around $\sim 80\%$ of WISSH QSOs, at projected distances of $\sim 6-130$ kpc. We observe a variety of sizes for the molecular gas reservoirs ($\sim 1.7-10$ kpc), mostly associated with rotating disks with disturbed kinematics. WISSH QSOs typically show lower CO luminosity and higher star formation efficiency than far-infrared matched, $z \sim 0-3$ main-sequence galaxies, implying that, given the observed SFR $\sim 170-1100\ M_\odot$ yr^{-1}, molecular gas is converted into stars on $\lesssim 50$ Myr. Most targets show extreme dynamical to black-hole mass ratios $M_{\rm dyn}/M_{\rm BH} \sim 3-10$, two orders of magnitude smaller than local relations. The molecular gas fraction in the host-galaxies of WISSH is lower by a factor of $\sim 10-100$ than in star forming galaxies with similar M_*.

Conclusions. Our analysis reveals that hyper-luminous QSOs at Cosmic noon undergo an intense growth phase of both the central SMBH and of the host-galaxy. These systems pinpoint the high-density sites where giant galaxies assemble, where we show that mergers play a major role in

Выборка…

ID	RA	Dec	z_{SDSS}	Telescope	Transition	Beamsize arcsec^2	ν_{cont} GHz	$\sigma_{40\ km\ s^{-1}}$ mJy beam^{-1}	σ_{cont} mJy beam^{-1}
(1)	(2)	(3)	(4)	(5)	(6)	(7)	(8)	(9)	(10)
J0209−0005	02:09:50.71	−00:05:06.22	2.849	NOEMA	CO(5−4)	4.9×2.7	148.7	0.90	0.040
				JVLA	CO(1−0)	3.1×2.3	31.6	0.08	0.005
J0801+5210	08:01:17.82	+52:10:34.94	3.217	NOEMA	CO(5−4)	3.8×1.9	136.6	1.05	0.100
				JVLA	CO(1−0)	3.4×2.3	30.2	0.16	0.010
J1433+0227	14:33:52.21	+02:27:14.01	4.622	ALMA	[CII]	0.44×0.34	338.1	0.43	0.051
J1538+0855	15:38:30.49	+08:55:17.42	3.542	ALMA	CO(4−3)	1.1×0.7	94.3	0.49	0.028
J1549+1245	15:49:38.71	+12:45:09.25	2.386	ALMA	CO(4−3)	1.0×0.9	141.8	0.10	0.007
J1555+1003	15:55:14.86	+10:03:51.23	3.512	ALMA	CO(4−3)	1.0×0.7	94.30	0.57	0.028
J1639+2824	16:39:09.11	+28:24:47.16	3.786	ALMA	CO(4−3)	0.20×0.13	100.4	0.43	0.026
J1701+6412	17:01:00.60	+64:12:09.32	2.724	NOEMA	CO(5−4)	4.0×2.1	154.7	1.03	0.100
J1015+0020*	10:15:49.00	+00:20:20.03	4.400	ALMA	[CII]	0.22×0.18	357.3	0.19	0.040

* presented in Bischetti et al. (2018)

Table 1. Journal of observations. Columns give the following information: (1) SDSS ID, (2-3) celestial coordinates, (4) redshift based on SDSS DR12 (Alam et al. 2015), (5) observation telescope, (6) observed transition, (7) angular resolution, (8) observed continuum frequency, (9) rms sensitivity for a channel width of 40 km s^{-1}, and (10) continuum rms sensitivity.

Очень яркие!

2. Sample and Observations

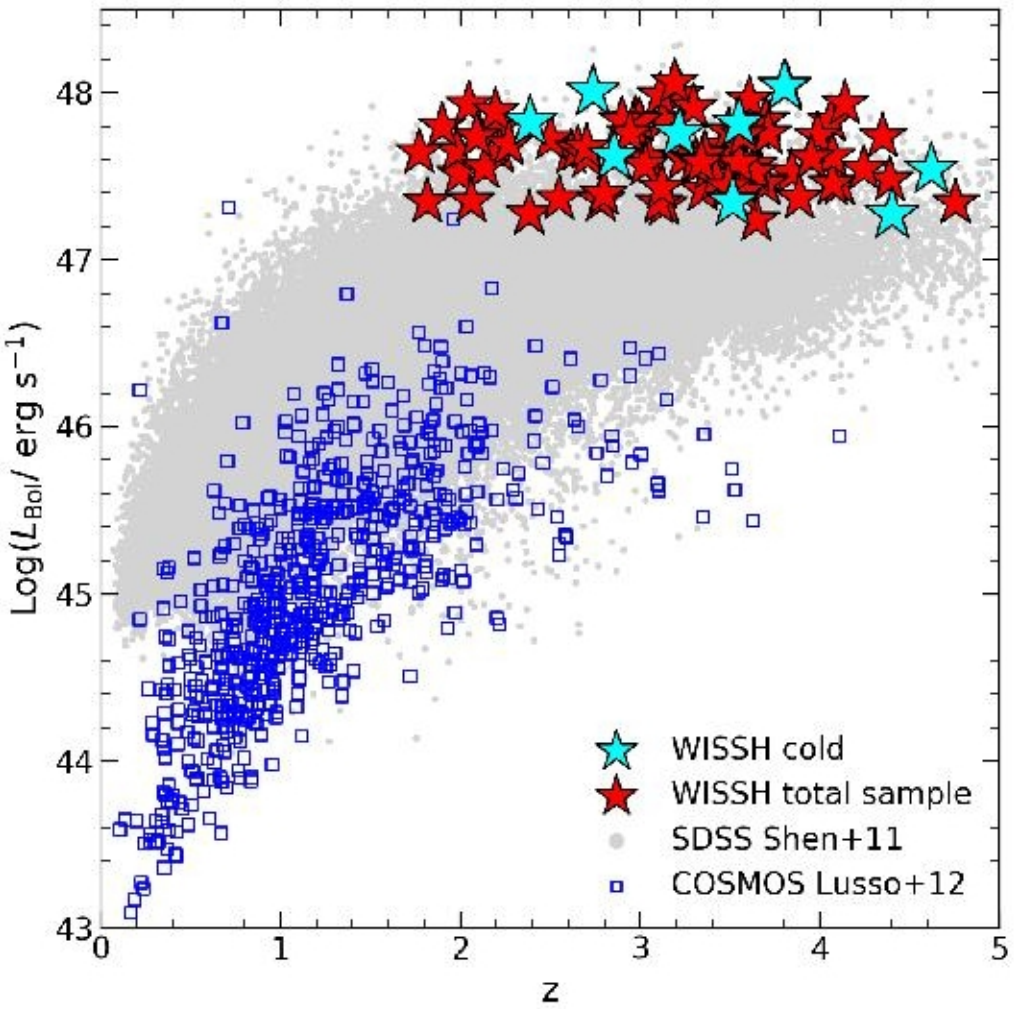

Молекулярный газ нашли везде

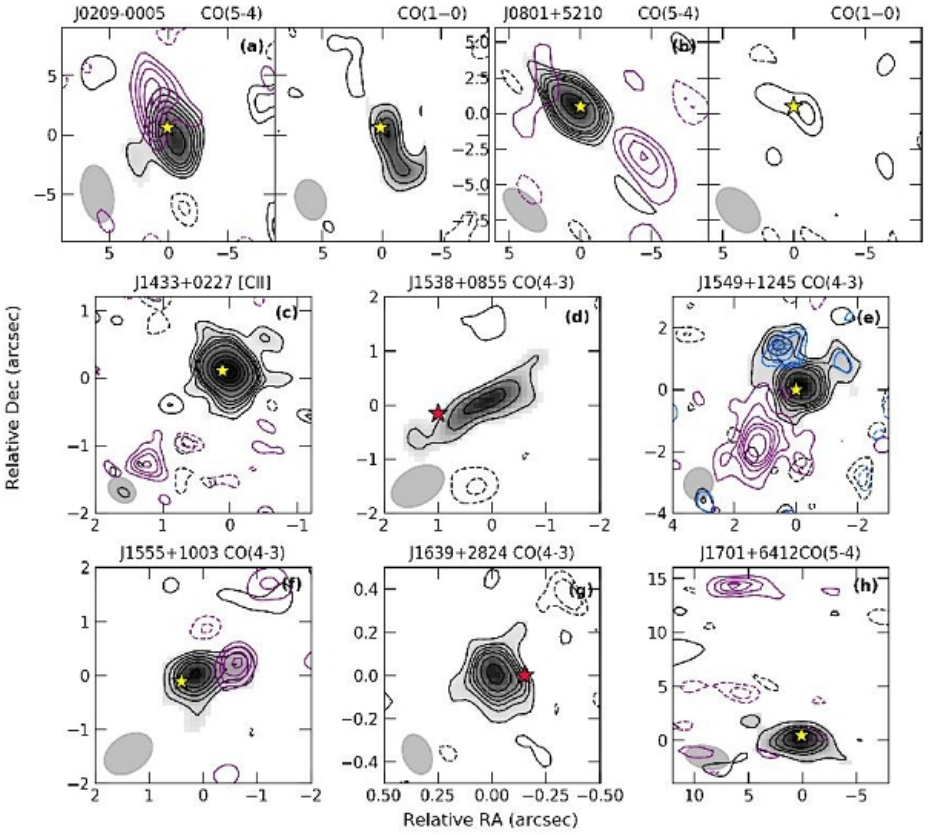

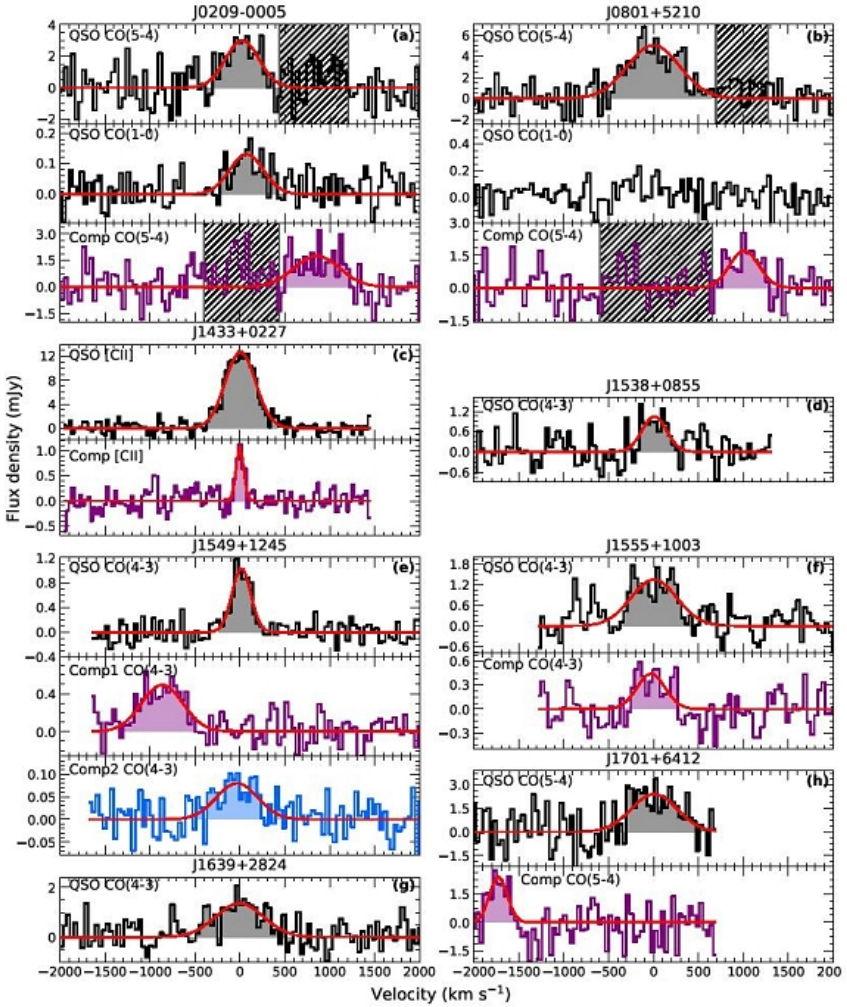

of the CO or [CII] emission lines for the WISSH QSOs analysed in this work. For each source, the targeted transi

Характеристики галактик – по SED

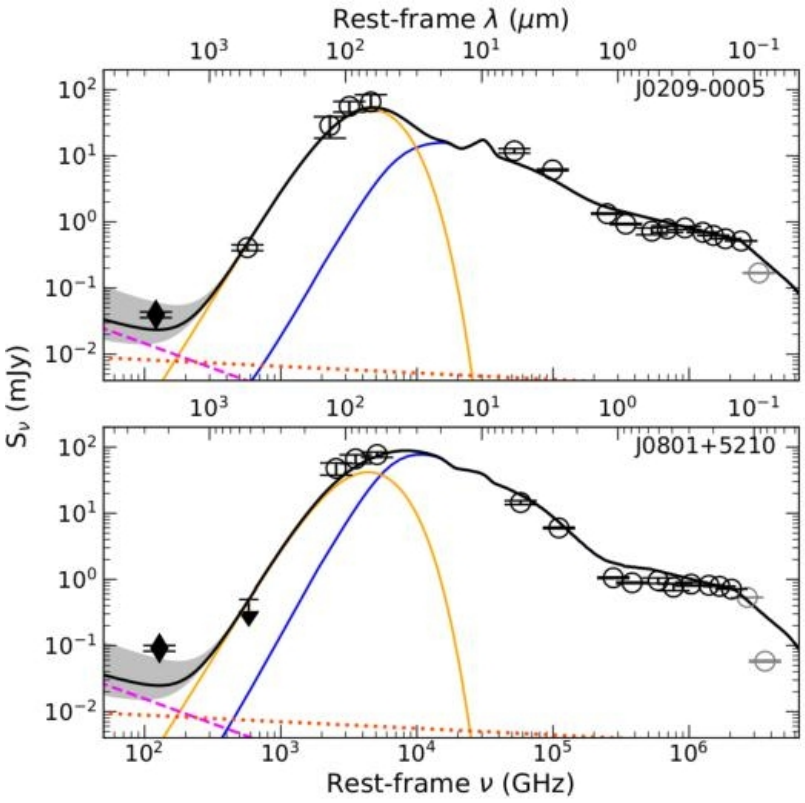

Fig. 6. Rest-frame SED of J0209−0005 (top) and J0801+5210 (bottom). In each panel, black circles indicate the photometric points considered (arrows represent 3σ upper limits). Photometric points at $\lambda < 1216$Å are not included in the fits due to Lyα absorption (grey circles). Rest-frame 125 GHz continuum data (not included in the fit) are shown by diamonds. Black curve represents the total best fit model, while blue(orange) curve refers to the QSO(cold dust) emission component. Synchrotron and free free emission are shown by the dashed and dotted lines, respectively.

Панорамная кинематика!

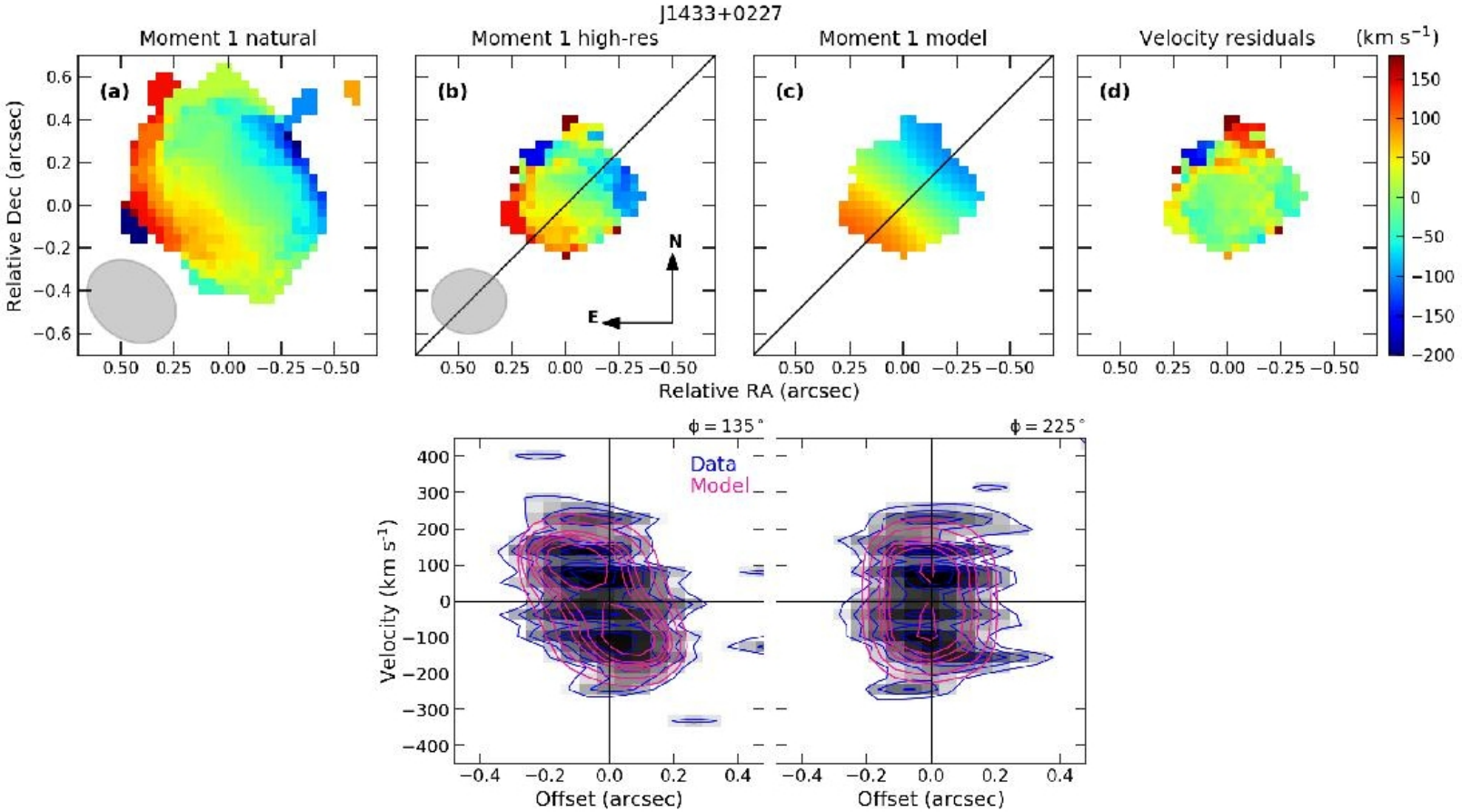

Не у всех, но есть

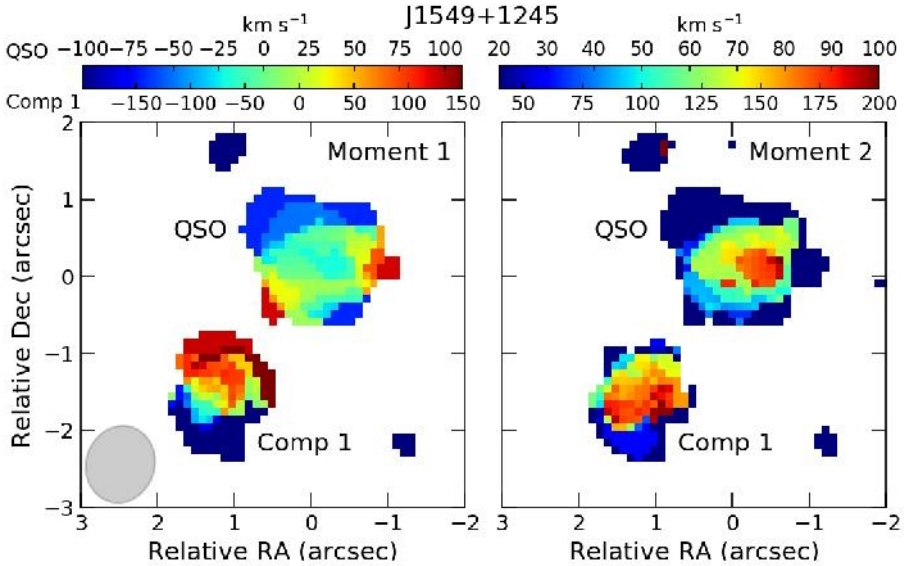

Fig. 8. Velocity (left) and velocity dispersion (right) maps of J1549+1245 and its bright companion, associated with CO(4−3) emission detected at > 3σ significance. In both panels, top(bottom) colorbar labels indicate values observed in the QSO(companion). The ALMA beam is also shown by the grey ellipse.

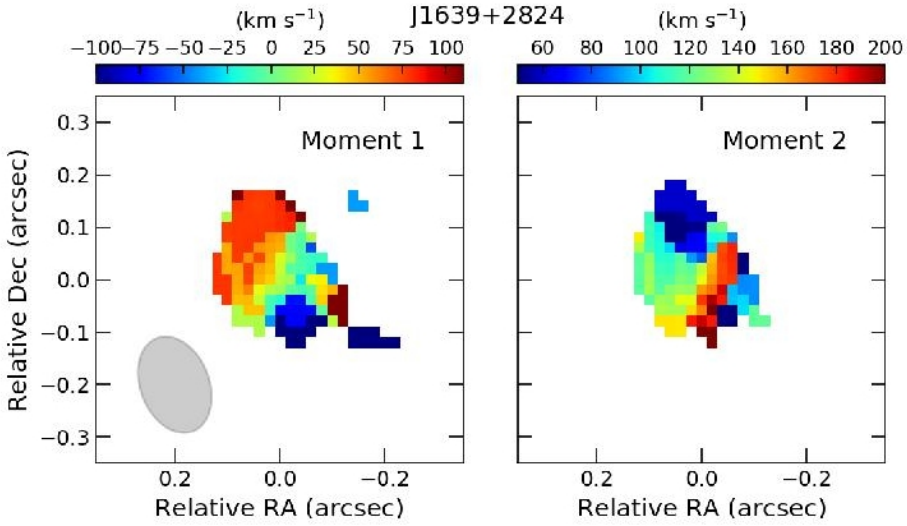

Fig. 9. Velocity (left) and velocity dispersion (right) maps of J1639+2824, associated with CO(4−3) emission detected at > 3σ significance. The ALMA beam is also shown by the grey ellipse.

Полученные характеристики

ID	log L_{FIR}	SFR	SFE	log M_{dust}	log M_{gas}	M_{gas}/M_{dust}	τ_{dep}
	$L_\odot$	$M_\odot$ yr^{-1}	$L_\odot$/(K km s^{-1} pc^2)	$M_\odot$	$M_\odot$		Myr
(1)	(2)	(3)	(4)	(5)	(6)	(7)	(8)
J0209−0005	13.17	735 [465−1165]	310 [230−415]	8.14	10.28±0.08	140	25 [15−40]
J0801+5210	13.24	875 [550−1385]	195 [150−250]	8.22	10.55±0.04	210	40 [25−65]
J1433+0227	12.74	270 [170−430]	–	8.74	11.00±0.30[b]	180[a]	360 [180−700]
J1538+0855	12.82	330 [165−660]	235 [120−470]	8.04	10.05±0.12	100	35 [15−65]
J1549+1245	12.52	165 [85−330]	305 [155−610]	7.64	9.64±0.04	100	25 [15−50]
J1555+1003	12.94	435 [220−870]	130 [65−260]	8.01	10.43±0.09	260	60 [30−120]
J1639+2824	12.72	260 [130−520]	65 [35−130]	8.04	10.51±0.07	300	125 [55−245]
J1701+6412	13.34	1095 [690−1735]	460 [340−625]	8.14	10.28±0.09	140	15 [10−25]
J1015+0020*	12.11	100 [65−160]	–	7.02	9.28±0.30[b]	180[a]	20 [10−45]

* presented in Bischetti et al. (2018)
[a] average value measured from WISSH QSOs with CO-based M_{gas}
[b] computed assuming $M_{gas}/M_{dust} = 180$

Table 3. Columns give the following information: (1) SDSS ID, (2) SED-based far-infrared luminosity (see Sect. 4) in the range $\lambda = 8 - 1000\ \mu$m. Typical uncertainty on L_{FIR} is 0.1 dex for sources with *Herschel* photometry, while for the other QSOs we consider a 0.3 dex error. (3-4) AGN-corrected SFR and star-formation efficiency, (5) dust mass, (6) molecular gas mass, (7) gas-to-dust ratio, and (8) molecular gas depletion time. In the last row we report the same quantities measured for J1015+0020, a WISSH QSO presented in Bischetti et al. (2018)

… мало газа при том же SFR!

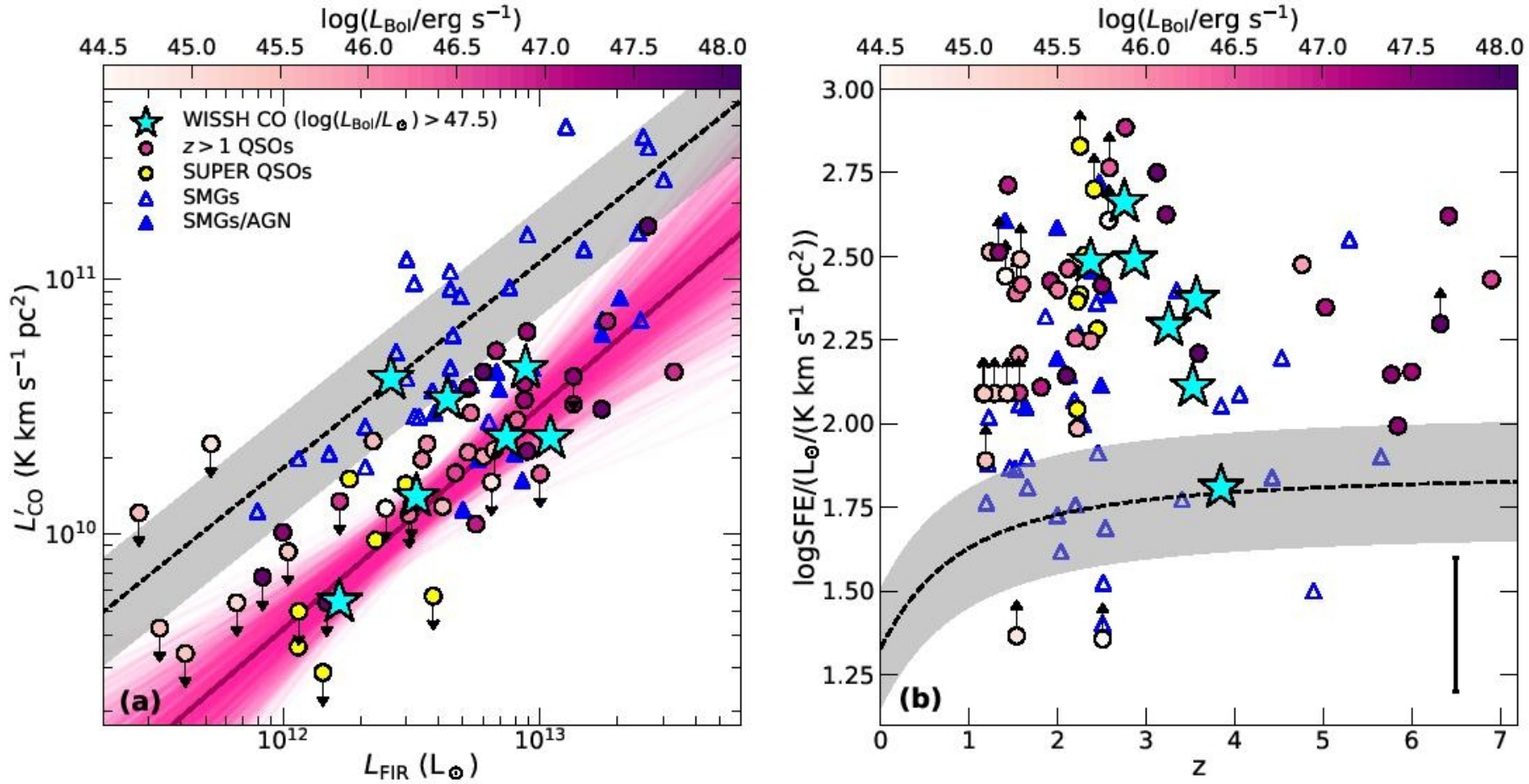

Ну, и слишком массивные дыры

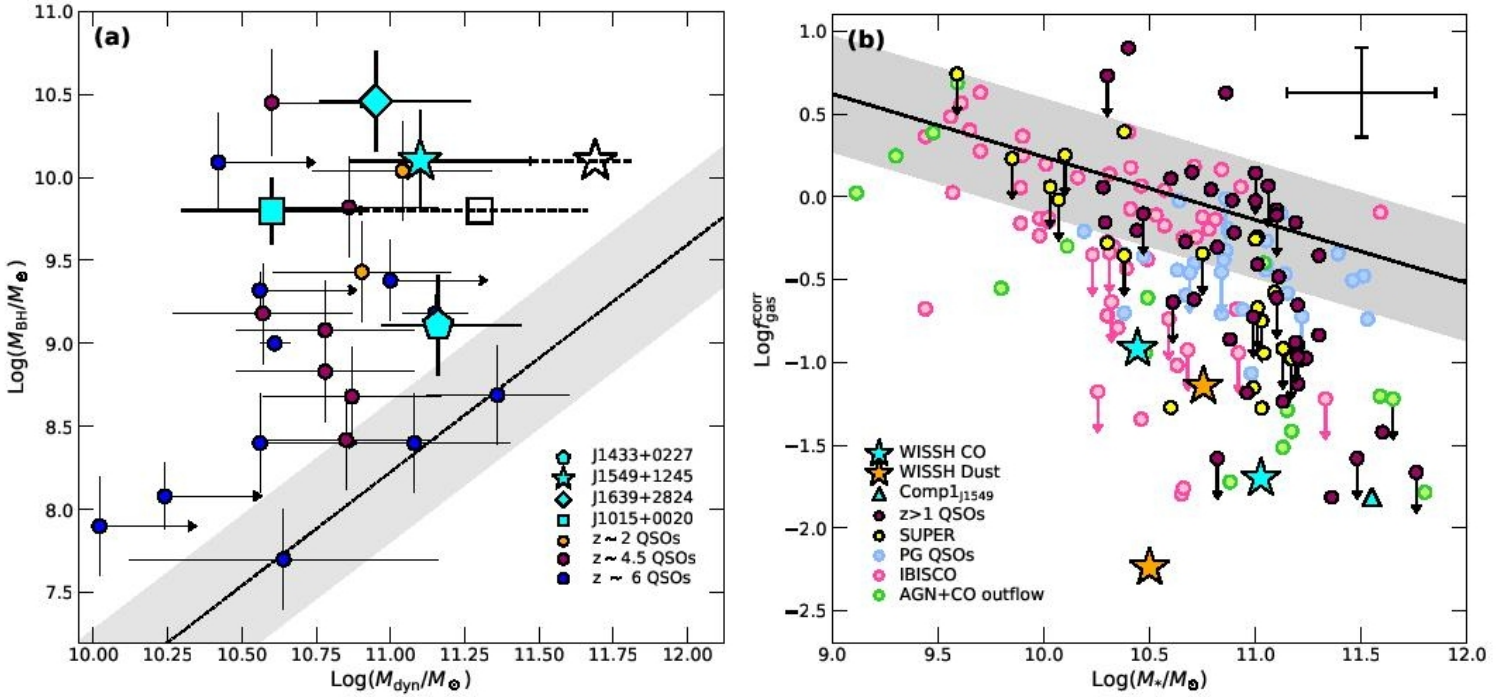

Fig. 11. Panel (a) shows the black hole mass as a function of the dynamical mass of WISSH QSOs (cyan symbols), compared with $z \sim 2-6$, luminous QSOs from literature, as indicated in the legend (see text for details). The total dynamical mass associated with the QSO + companion galaxies with measured M_{dyn} are also shown by the empty symbols. For WISSH QSOs and companions (as most literature sources), M_{dyn} values are based on the FWHM of the CO or [CII] emission lines. The $M_{BH} - M_{dyn}$ relation found for local galaxies by Jiang et al. (2011) is also indicated by the dashed line, with the associated 0.4 dex intrinsic scatter (shaded region). Panel (b) displays the molecular gas fraction (corrected for the dependence on redshift and offset from main-sequence) as a function of the host-galaxy stellar mass for WISSH QSOs and a compilation of high-z QSOs and local AGN (see text). WISSH QSOs with dust-based M_{gas} are indicated by orange stars. The average $f_{gas} - M_*$ relation found for $z < 4$ star-forming galaxies from the PHIBSS survey (Tacconi et al. 2018) is shown by the solid line. The typical uncertainty on f_{gas} (due to different

ArXiv:2009.01277

The rocky road to quiescence: compaction and quenching of quasar host galaxies at z ~ 2

H. R. Stacey,[1,2,3]★ J. P. McKean,[1,2] D. M. Powell,[3] S. Vegetti,[3] F. Rizzo,[3] C. Spingola,[4,5] M. W. Auger,[6,7] R. J. Ivison[8] and P. P. van der Werf[9]

[1]*ASTRON, Netherlands Institute for Radio Astronomy, Oude Hoogeveensedijk 4, 7991 PD, Dwingeloo, The Netherlands*
[2]*Kapteyn Astronomical Institute, University of Groningen, PO Box 800, 9700 AV Groningen, The Netherlands*
[3]*Max Planck Institute for Astrophysics, Karl-Schwarzschild Str. 1, D-85748 Garching bei München, Germany*
[4]*INAF – Istituto di Radioastronomia, Via Gobetti 101, I–40129, Bologna, Italy*
[5]*Dipartimento di Fisica e Astronomia, Università degli Studi di Bologna, Via Gobetti 93/2, I–40129 Bologna, Italy*
[6]*Institute of Astronomy, University of Cambridge, Madingley Road, Cambridge CB3 0HA, UK*
[7]*Kavli Institute for Cosmology, University of Cambridge, Madingley Road, Cambridge CB3 0HA, UK*
[8]*European Southern Observatory, Karl-Schwarzschild-Str. 2, D-85748 Garching bei München, Germany*
[9]*Leiden Observatory, Leiden University, PO Box 9513, NL-2300 RA Leiden, The Netherlands*

Accepted XXX. Received YYY; in original form ZZZ

ABSTRACT

We resolve the host galaxies of seven gravitationally lensed quasars at redshift 1.5 to 2.8 using observations with the Atacama Large (sub-)Millimetre Array. Using a visibility-plane

Опять выборка…

Table 1. Summary of the targets and ALMA observations. We give the phase centre right ascension and declination (in degrees, J2000), lens and source redshift (from optical spectroscopy – improved redshift estimates for these systems are presented in Table 2), central frequency of the observation, total on-source integration, the FWHM of the naturally weighted beam, and project code for the seven targets in this work. The redshift of the lens is not known for HS 0810+2554, H1413+117 or WFI J2026−4536, but this has no bearing on our results.

	RA (deg)	Dec (deg)	z_l	z_s	ν_{obs} (GHz)	t_s (min)	FWHM (arcsec)	Project code
HS 0810+2254	123.38053	+25.75068	–	1.51	145 GHz	32	0.17×0.13	2017.1.01368.S
RX J0911+0551	137.86458	+05.84833	0.70	2.79	145 GHz	123	0.40×0.35	2017.1.01081.S
SDSS J0924+0219	141.23258	+02.32347	0.39	1.52	358 GHz	44	0.28×0.23	2018.1.01591.S
PG 1115+080	169.57083	+07.76603	0.31	1.74	346 GHz	27	0.32×0.21	2018.1.01591.S
H1413+117	213.94271	+11.49539	–	2.56	285 GHz	10	0.24×0.21	2012.1.00175.S
WFI J2026−4536	306.54346	−45.60753	–	2.22	350 GHz	28	0.14×0.14	2018.1.01591.S
WFI J2033−4723	308.42533	−47.39528	0.66	1.66	341 GHz	28	0.31×0.28	2018.1.01591.S

И опять газ (почти) везде.

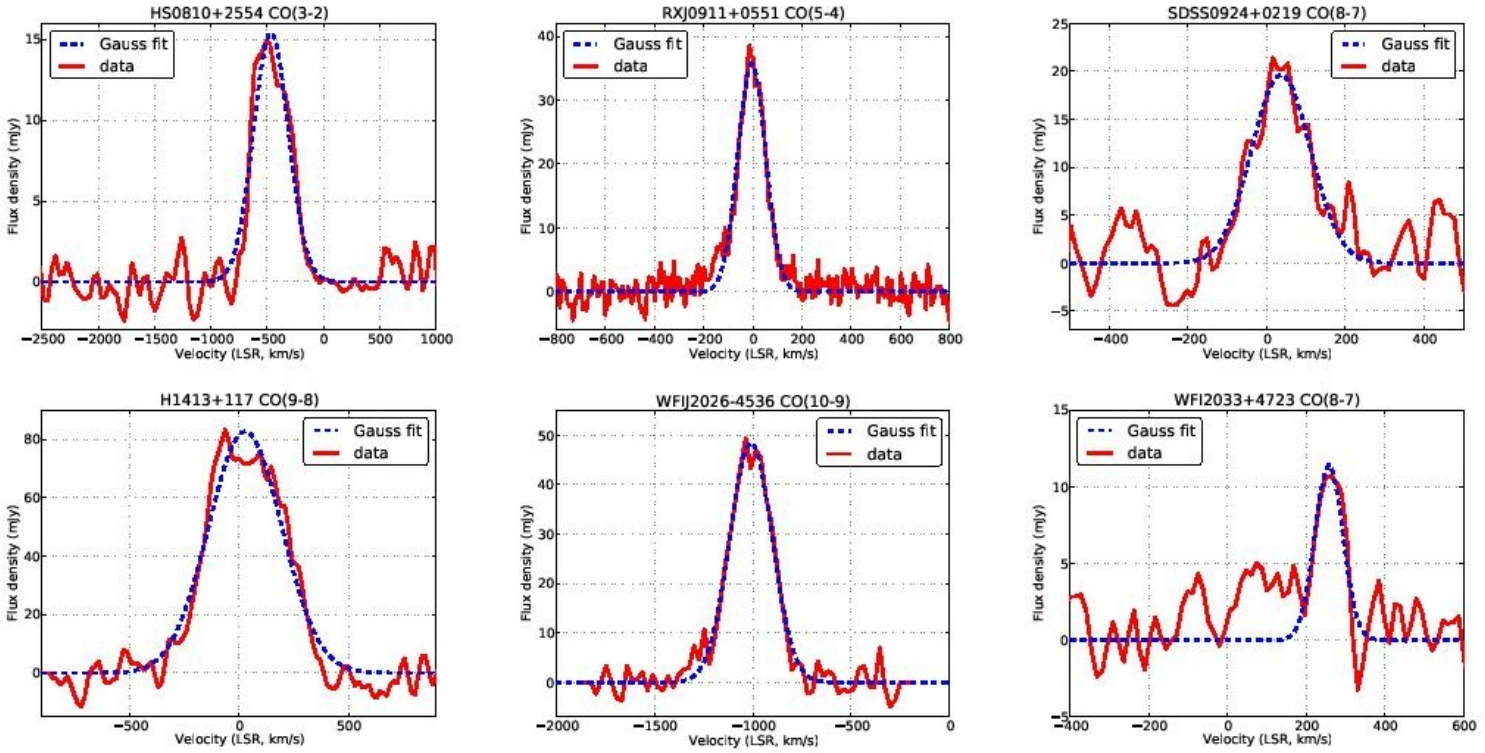

Figure 1. Line profiles for the six objects with CO observations. The red line shows the data; the blue dotted line is a Gaussian fit to the data. The systemic velocity is relative to the best redshift from the literature, using the radio definition of velocity.

Пример: HS0810+2554

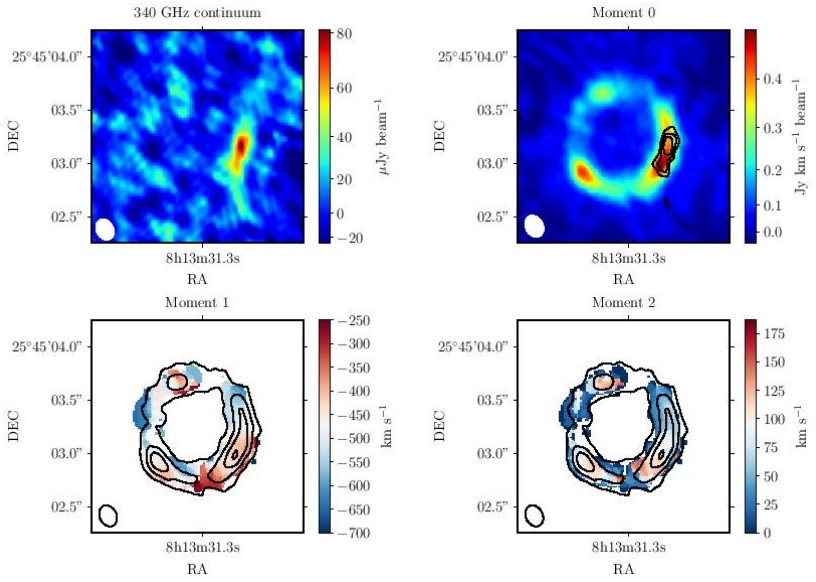

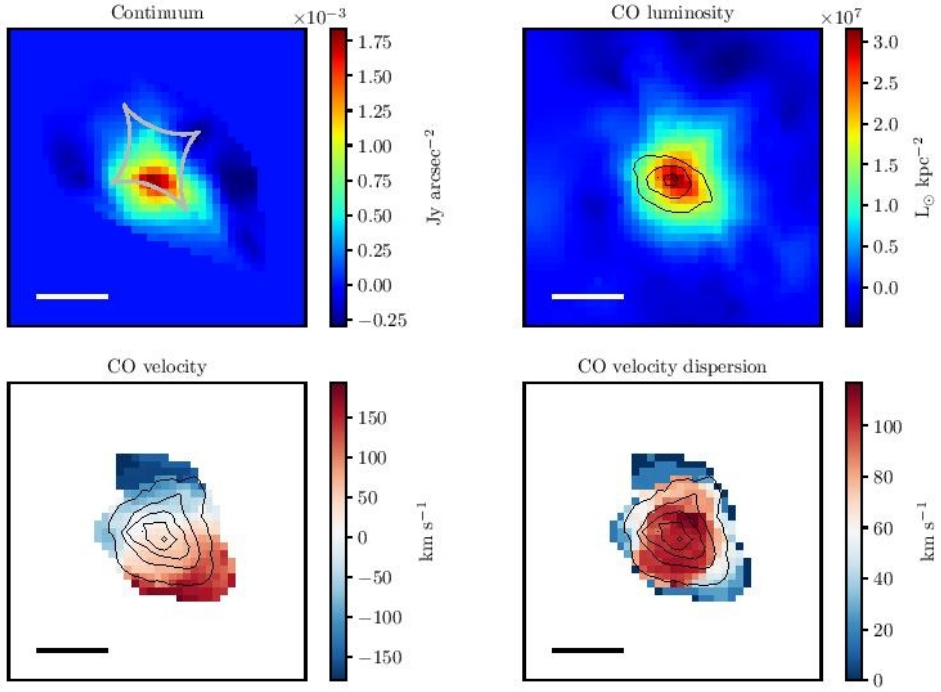

Пример: H1413+117

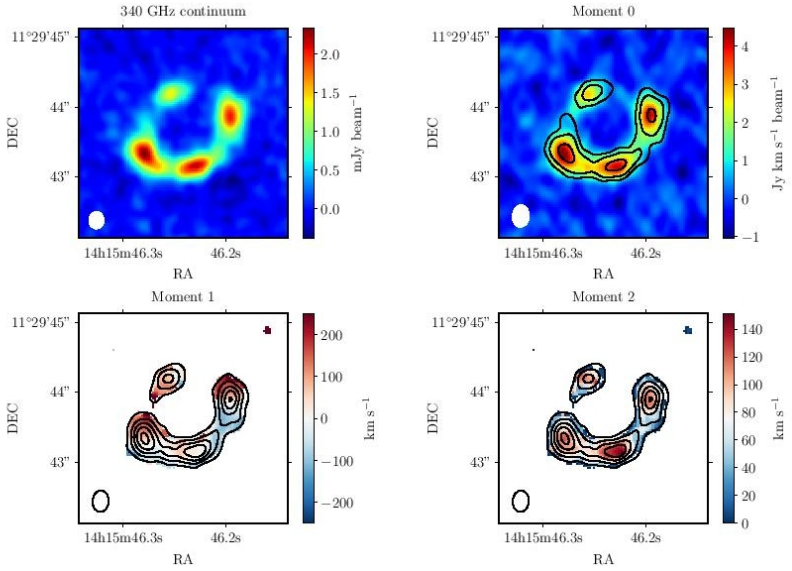

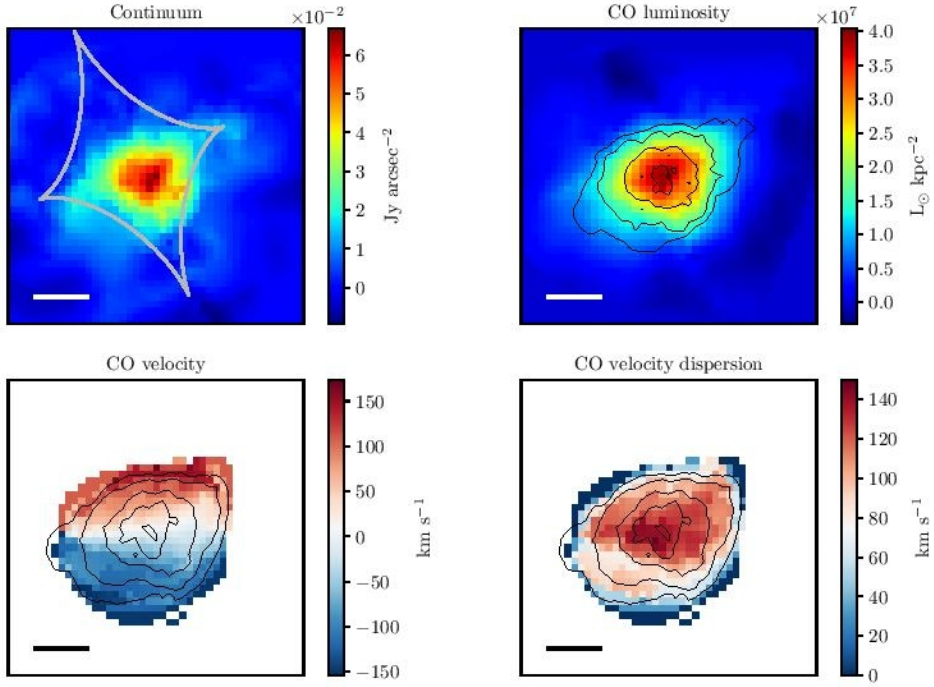

Результаты: пыль

Table 4. The properties of the reconstructed continuum emission, corrected for lensing magnification. For H1413+117 we give values after correcting the SED for photometri
for all except WFI J2033−4723 and PG 1115+080, the quoted sizes include an additional ±10% uncertainty due to empirical scatter in the slope of the mass profile (see Secti

	$\mu_{\rm dust}$	$R_{\rm dust}$ (kpc)	n	$T_{\rm d}^{\rm cold}$ (K)	$T_{\rm d}^{\rm warm}$ (K)	β	$L_{\rm FIR}$ ($L_\odot$)	SFR ($M_\odot$ yr^{-1})	$\Sigma_{\rm SFR}$ ($M_\odot$ yr^{-1} kpc^{-2})
HS 0810+2554	24 ± 4	0.46 ± 0.10	0.57 ± 0.05	39^{+4}_{-5}	135^{+25}_{-18}	$\equiv 2$	$8^{+5}_{-5} \times 10^{11}$	45^{+35}_{-30}	40^{+30}_{-30}
RX J0911+0551	10.6 ± 0.2	0.54 ± 0.06	0.56 ± 0.04	54^{+3}_{-3}	–	$1.9^{+0.1}_{-0.1}$	$1.8^{+0.2}_{-0.2} \times 10^{12}$	600^{+80}_{-70}	300^{+70}_{-70}
SDSS J0924+0219	15.1 ± 0.7	1.9 ± 0.2	1.2 ± 0.1	38^{+8}_{-7}	–	$1.5^{+0.6}_{-0.4}$	$2.7^{+0.9}_{-0.7} \times 10^{11}$	90^{+30}_{-20}	5^{+2}_{-2}
PG 1115+080	14.6 ± 0.4	0.35 ± 0.04	0.47 ± 0.01	66^{+17}_{-21}	–	$1.9^{+0.3}_{-0.3}$	$3.6^{+1.6}_{-1.3} \times 10^{11}$	120^{+50}_{-40}	310^{+150}_{-125}
H1413+117	11.2 ± 0.2	0.9 ± 0.1	0.66 ± 0.07	53^{+1}_{-1}	246^{+14}_{-24}	$1.88^{+0.04}_{-0.04}$	$4.9^{+0.6}_{-0.6} \times 10^{12}$	1600^{+200}_{-200}	290^{+80}_{-80}
WFI J2026−4536	19.6 ± 0.8	0.31 ± 0.03	0.61 ± 0.02	63^{+4}_{-3}	–	$1.8^{+0.1}_{-0.1}$	$3.1^{+1.7}_{-1.5} \times 10^{12}$	1010^{+60}_{-50}	2200^{+900}_{-900}
WFI J2033−4723	17.6 ± 0.9	2.5 ± 0.2	1.1 ± 0.2	31^{+7}_{-5}	–	$1.7^{+0.3}_{-0.3}$	$4.6^{+1.3}_{-1.0} \times 10^{11}$	150^{+40}_{-30}	3^{+1}_{-1}

Результаты: газ

Table 5. The properties of the reconstructed CO line emission, corrected for lensing magnification. For SDSS J0924+0219 and WFI J2033−4723, the Sérsic index, n, is fixed found for the dust continuum). All parameters are derived from moment maps of the reconstructed source. Note that for all except WFI J2033−4723 and PG 1115+080, the c uncertainty due to empirical scatter in the slope of the mass profile (see Section 4.1 for details).

	$\tilde{\mu}_{CO}$	R_{CO} (kpc)	n	I_{CO} (Jy km s^{-1})	L_{CO} ($L_\odot$)	L'_{CO} (K km s^{-1} pc^2)	M_{dyn} ($M_\odot$)
HS 0810+2554	20.3 ± 0.7	0.52 ± 0.03	0.57 ± 0.06	0.19 ± 0.01	$(3.4 \pm 0.1) \times 10^6$	$(2.6 \pm 0.1) \times 10^9$	$(3.5 \pm 2.1) \times 10^{10}$
RX J0911+0551	10.3 ± 0.2	0.7 ± 0.1	0.56 ± 0.01	0.47 ± 0.01	$(4.2 \pm 0.1) \times 10^7$	$(6.9 \pm 0.1) \times 10^9$	$(1.2 \pm 0.6) \times 10^9$
SDSS J0924+0219	17 ± 1	1.5 ± 0.4	$\equiv 1.0$	0.13 ± 0.01	$(6.4 \pm 0.4) \times 10^6$	$(2.5 \pm 0.2) \times 10^8$	$(1.0 \pm 0.5) \times 10^{10}$
H1413+117	11.1 ± 0.2	0.9 ± 0.1	0.54 ± 0.05	3.4 ± 0.1	$(4.8 \pm 0.1) \times 10^8$	$(1.34 \pm 0.02) \times 10^{10}$	$(2.4 \pm 0.4) \times 10^{10}$
WFI J2026−4536	19.6 ± 0.8	0.31 ± 0.03	0.52 ± 0.03	0.54 ± 0.02	$(6.6 \pm 0.3) \times 10^7$	$(1.4 \pm 0.1) \times 10^9$	$(4.0 \pm 0.3) \times 10^9$
WFI J2033−4723	17 ± 2	1.4 ± 0.3	$\equiv 1.0$	0.026 ± 0.003	$(1.5 \pm 0.2) \times 10^6$	$(6.1 \pm 0.7) \times 10^7$	$(2.1 \pm 1.2) \times 10^9$

Нагретая пыль в 5 случаях из 7 очень компактна!

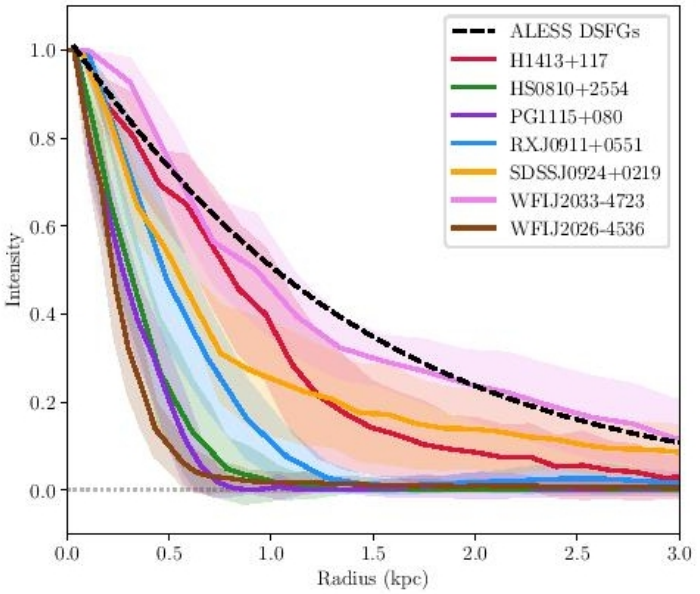

Figure 17. Normalised, azimuthally averaged surface brightness profiles of the reconstructed dust emission from the quasar hosts, accounting for ellipticity. The shaded regions show the respective standard deviation of the dust emission. The radius of HS 0810+2554, RX J0911+0551 and PG 1115+080 are scaled to the size of the minor axis, based on the axis ratio from the Sérsic model fits (see Section 4.1). The black dotted line shows the mean profile of (unlensed) ALESS DSFGs from Sérsic fits (Hodge et al. 2016, 2019).

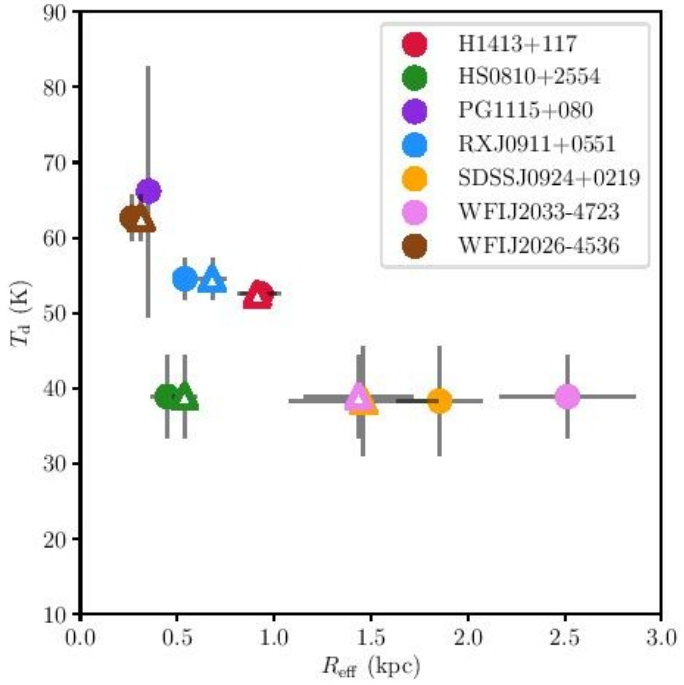

Figure 18. The effective radius (R_{eff}) of the dust continuum (solid circles) and CO line emission (open triangles) against effective dust temperature (T_d) for the seven lensed quasar hosts investigated here.

Снова мало газа и короткое время исчерпания

HS 0810+2554 is the only object where we observe CO (3–2), which is a common proxy for molecular hydrogen (H_2; Greve et al. 2014). We assume $\alpha_{CO} = 0.8\ M_\odot\ (K\ km\ s^{-1}\ pc^2)^{-1}$, as is often assumed for dusty starbursts, to convert L'_{CO} to total gas mass (M_{gas}). For this object we find $M_{gas} = (2.1 \pm 0.1) \times 10^9\ M_\odot$ and $\Sigma_{gas} = 1.6 \pm 0.7\ M_\odot\ kpc^{-2}$ (derived in the same manner as Eq. 7). This implies a very low gas fraction of just 0.06 ± 0.04 compared to its dynamical mass, and a dust-to-gas ratio is 0.006 ± 0.002 (slightly below solar metallicity). The implied gas depletion timescale (i.e. $t_{dep} \equiv M_{gas}/SFR$) is 50 ± 40 Myr.

Неожиданный вывод: звездообразование останавливает оно же само, а не квазар!

Эддингтон!